electronics

MDPI

Article

Intelligent Degradation-Aware Dispatch for Inverter-Based Photovoltaic–Battery Energy Systems

Adewale Ogabi, Geetika Aggarwal *, Palat Meethale Ushasree and Gobind Pillai

School of Computing, Engineering, & Digital Technologies, Teesside University, Middlesbrough TS1 3BX, UK; hello@adewaleogabi.info (A.O.); p.ushasree@tees.ac.uk (P.M.U.); g.g.pillai@tees.ac.uk (G.P.)
* Correspondence: g.aggarwal@tees.ac.uk

Abstract

Solar photovoltaic (PV) and battery energy storage systems (BESS) are increasingly deployed in homes and communities. However, conventional operational strategies often prioritise short-term electricity costs without considering equipment ageing. Repeated battery cycling contributes to capacity degradation, while temperature-dependent PV losses affect available generation and system efficiency. This study develops an intelligent degradation-aware dispatch framework for inverter-interfaced PV–battery systems, integrating reduced-order battery ageing, PV degradation and thermal derating, inverter constraints, and adaptive supervisory control within a lightweight, rule-based architecture. The framework assesses electricity-cost and battery-preservation trade-offs under operating constraints. A full-year simulation at 15 min resolution compares four policies: Baseline, Battery-Aware, Battery+PV-Aware, and Adaptive-Supervisory. Relative to the Baseline, Battery-Aware and Battery+PV-Aware reduce annual equivalent full cycles (EFCs) by 18.03% and 29.10%, respectively, with electricity-cost changes of −0.11% and +1.88%. The Adaptive-Supervisory policy reduces EFCs by 8.49% and operating cost by 1.81%. Controlled ablations show that supervisory adaptation reduces cycling by 2.14% and 10.15% under supplementary synthetic tariffs, but does not alter dispatch under the original three-level tariff. Equal-constraints comparisons further reveal tariff-dependent trade-offs between fixed and adaptive degradation weighting, without establishing universal adaptive superiority. Supplementary simulations using UK-DALE residential demand and PVGIS meteorological inputs show consistent battery-cycling reductions of 19.27–20.67% over 198.25 days. The findings demonstrate that degradation-informed policies can reduce battery cycling with modest economic trade-offs, while adaptive supervision provides additional benefits under suitable tariff conditions. The framework offers a transparent, computationally tractable approach to lifecycle-aware energy management, with physical validation and calibrated ageing models remaining priorities for future work.

Keywords: intelligent energy management; inverter-based systems; photovoltaic–battery systems; degradation-aware dispatch; battery energy storage; adaptive control; renewable energy integration

Check for updates

Academic Editors: Yuan Yan, Le Liu and Min Wu

Received: 21 September 2026
Revised: 15 October 2026
Accepted: 22 October 2026
Published: 24 October 2026

Copyright: © 2026 by the authors. Licensee MDPI, Basel, Switzerland. This article is an open access article distributed under the terms and conditions of the Creative Commons Attribution (CC BY) license.

1. Introduction

The transition to renewable energy is accelerating the deployment of solar photovoltaic (PV) and battery energy storage systems (BESS) in residential, community, and small-scale industrial applications. These systems can reduce electricity costs, improve grid flexibility, and support emissions reduction [1–5]. The addition of global renewable capacity exceeded

510 GW in 2023, primarily driven by the expansion of solar PV power [6–8]. Battery storage deployment is also expected to grow substantially, supporting renewable integration, resilience, and system flexibility [9], with recent reviews highlighting significant growth towards 2030 [10–12]. Coordinating PV generation and battery storage therefore presents an important control challenge in distributed energy systems, where dispatch decisions affect efficiency, asset utilisation, and reliability [13]. As both resources interface with electrical networks through power electronic converters, these decisions also determine active-power references and operating conditions of inverter-interfaced resources.

Recent research on inverter-based resources has also addressed system-level stability through frequency-spectra impedance analysis, including the identification of weak points of interconnection [14]. While such studies focus on electrical stability, the present work examines operational cost and degradation-related dispatch trade-offs in PV–battery systems.

Conventional energy-management strategies often prioritise short-term economic objectives, including tariff arbitrage, peak shaving, and self-consumption, without fully considering equipment ageing. Battery capacity deteriorates through calendar and cycle ageing, influenced by temperature, state of charge, depth of discharge, and operating time [15–17]. PV modules also experience performance losses associated with light-induced degradation (LID), potential-induced degradation (PID), and environmental stressors, with rates varying across technologies and operating conditions [18–20]. Although these processes occur over different timescales, they affect available energy, battery utilisation, and system economics. Neglecting degradation-related effects may therefore favour immediate financial returns at the expense of longer-term asset performance.

Recent studies have incorporated battery degradation into energy-management and scheduling frameworks through degradation-cost formulations, constrained optimisation, and predictive control [21–23]. Digital-twin-inspired methods and intelligent supervisory strategies have also supported monitoring, performance assessment, and operational decisions [24–26]. However, integrating battery ageing indicators, temperature-dependent PV performance, inverter constraints, and adaptive supervision within a transparent, computationally lightweight framework remains a practical challenge. Importantly, the effects of degradation-informed policies must be distinguished from changes in battery operating limits and tariff thresholds, while the additional contribution of adaptive supervision requires evaluation under varying operating conditions.

From an energy conversion and management perspective, equipment ageing also affects the economic and environmental implications of asset replacement [27,28]. Battery replacement and PV maintenance can increase material demand and lifecycle impacts associated with manufacturing, transportation, and end-of-life management [29–32]. These considerations motivate energy-management strategies that balance degradation-related performance with operating costs. Nevertheless, simulated cycling reductions do not establish experimentally verified lifetime extension or quantified environmental benefits. Evaluating these trade-offs can inform more resource-conscious and economically efficient PV–battery operation.

2. Literature Review

Research on PV–battery systems encompasses economic dispatch, ageing models, lifecycle assessment, digital twins, and artificial intelligence [33–40]. Operational strategies commonly address peak shaving, tariff arbitrage, and self-consumption through model predictive control (MPC), linear programming, and heuristic methods [1,41–43]. Although effective for economic scheduling, their treatment of asset ageing varies, potentially overlooking longer-term degradation-related costs.

Battery degradation arises from calendar and cycle ageing, with rainflow counting widely used to characterise cycling stress [44,45]. Detailed electrochemical models offer physical fidelity but require substantial calibration and computational resources [46,47]. Reduced-order ageing models and degradation-cost formulations have therefore been incorporated into operational scheduling [45,48–50]. Similarly, PV degradation studies document long-term performance changes across technologies and climates [5,19,20,51]. While irradiance and temperature are routinely represented in generation models, prescribed PV ageing is less consistently integrated into operational assessments and should not be confused with dispatch-controllable degradation. Lifecycle methods, including levelised cost of energy (LCOE) and storage (LCOS), complement these models by assessing investment, replacement, and long-term operating costs [32,52–55].

Digital twin approaches support energy-system monitoring, performance assessment, predictive maintenance, and decision-making [24,25], including applications in microgrid management and supervisory control [56,57]. However, simulation-based digital counterparts must be distinguished from operational twins incorporating live physical-system synchronisation. Artificial intelligence and deep reinforcement learning (DRL) have also been applied to energy management under variable demand, generation, and tariffs [12,58–61]. Although these approaches may incorporate degradation penalties and operating constraints, their effectiveness depends on model formulation, training requirements, and computational resources. Deterministic hierarchical control remains relevant where transparent supervisory decisions and explicit inverter and battery constraints are priorities.

Recent energy storage and energy conversion studies have advanced digital twin modelling, battery degradation assessment, and ageing-aware optimisation [62–67]. Nevertheless, a practical evaluation challenge remains in integrating reduced-order battery ageing, prescribed PV performance degradation, inverter constraints, and adaptive supervision within a transparent dispatch framework. In particular, controlled comparisons are needed to distinguish the contribution of adaptive mechanisms from policy-specific operating limits and to examine performance under alternative operating inputs.

Table 1 compares representative studies across dispatch decision-making (DD), battery ageing (BA), PV degradation (PVD), digital-twin monitoring (DT-M), operational decision support (DT-O), lifecycle cost modelling (LCO), learning-based AI control (DRL/AI), and hardware-in-the-loop validation (HIL). The comparison identifies the modelling and operational dimensions addressed by existing approaches. This study combines degradation-informed, inverter-constrained dispatch with fixed-policy comparisons, controlled supervisory ablations, and supplementary measured-input evaluation.

Table 1. Comparison of selected modelling and operational dimensions across representative studies and the proposed framework (Y: yes; N: no; P: partial).

Literature	DD	BA	PVD	DT-M	DT-O	LCO	DRL/AI	HIL
[24,25]	N	N	N	Y	N	N	N	N
[45,48,68–71]	Y	Y	N	N	P	P	P	N
[19,20,51]	N	N	Y	N	N	N	N	N
[72–74]	Y	Y	N	N	Y	P	P	N
[56,57,75,76]	Y	P	N	P	Y	P	P	N
[58–61]	Y	P	N	N	Y	N	Y	N
This study	Y	Y	Y	P	P	P	N	N

Novelty and Contributions

This study contributes an intelligent degradation-aware dispatch framework for inverter-interfaced photovoltaic–battery energy systems, integrating battery ageing indicators, temperature-dependent PV performance, and inverter operating constraints within a unified energy-management architecture. Building on established degradation models and heuristic dispatch principles, the contribution lies in their transparent integration and comparative evaluation rather than the development of new ageing physics or a numerical optimisation algorithm. Battery degradation is represented through a marginal discharge-cost penalty, while PV ageing and thermal derating are incorporated into the available generation model and performance assessment. This distinction enables degradation-related operating effects to be examined without implying active control of the underlying PV ageing process.

A lightweight adaptive supervisory layer adjusts the battery degradation weight and discharge threshold according to normalised operating stress indicators, including state of charge, temperature, load demand, and electricity price. The lower-level deterministic controller enforces power balance, battery operating limits, and inverter constraints. Beyond comparing fixed and adaptive dispatch policies, the study employs controlled supervisory ablations under different tariff conditions to distinguish the effects of adaptive mechanisms from those of policy-specific operating thresholds and constraints. Supplementary evaluation using measured residential demand and historical meteorological inputs further examines the consistency of the resulting battery-cycling trends beyond the primary synthetic simulation.

Figure 1 illustrates the conceptual structure of the proposed degradation-aware, digital-twin-inspired framework. The simulated PV–battery system is represented through interconnected power-conversion, energy-storage, degradation, and supervisory decision models. A user-facing interaction layer supports scenario exploration and interpretation of operational and degradation-related indicators. Dispatch calculations are executed automatically through the rule-based controller, providing a transparent and computationally lightweight decision-support environment. The present implementation does not incorporate live physical-system synchronisation or bidirectional hardware interaction and is therefore positioned as a simulation-based digital counterpart rather than a fully deployed physical digital twin.

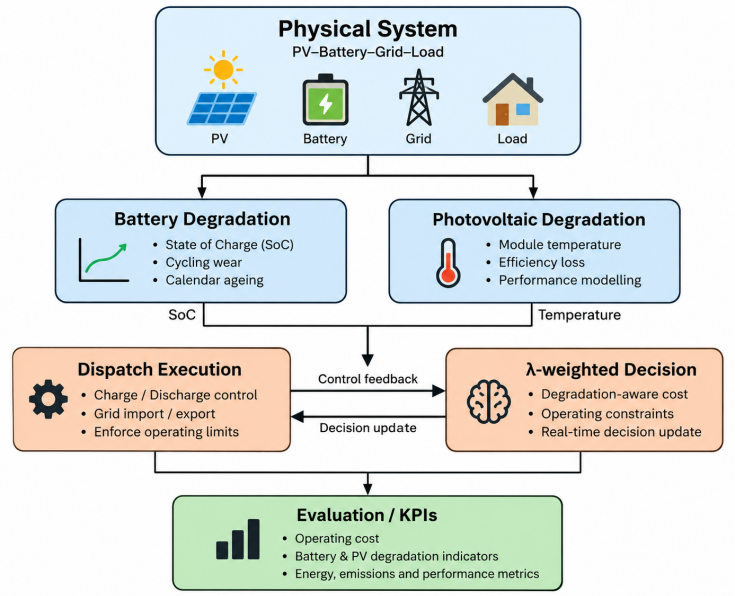


Figure 1. Conceptual overview of the proposed degradation-aware supervisory dispatch framework.

3. Methodology

The proposed framework implements degradation-aware supervisory dispatch for an inverter-interfaced PV–battery energy system. The computational architecture combines (i) a physics-based operational system model, (ii) reduced-order battery and PV degradation models, and (iii) a weighted supervisory decision layer that incorporates ageing-related indicators into dispatch decisions. The structure is designed for short-interval operational energy management while maintaining low computational complexity and transparent degradation accounting. This approach is consistent with recent degradation-aware energy management studies [72,77,78].

Figure 2 illustrates the interaction between the physical system layer, the degradation evaluation layer, and the operational decision logic. In contrast to planning-oriented optimisation frameworks, the proposed supervisory dispatch framework operates at short control intervals and updates degradation indicators alongside system power flows.

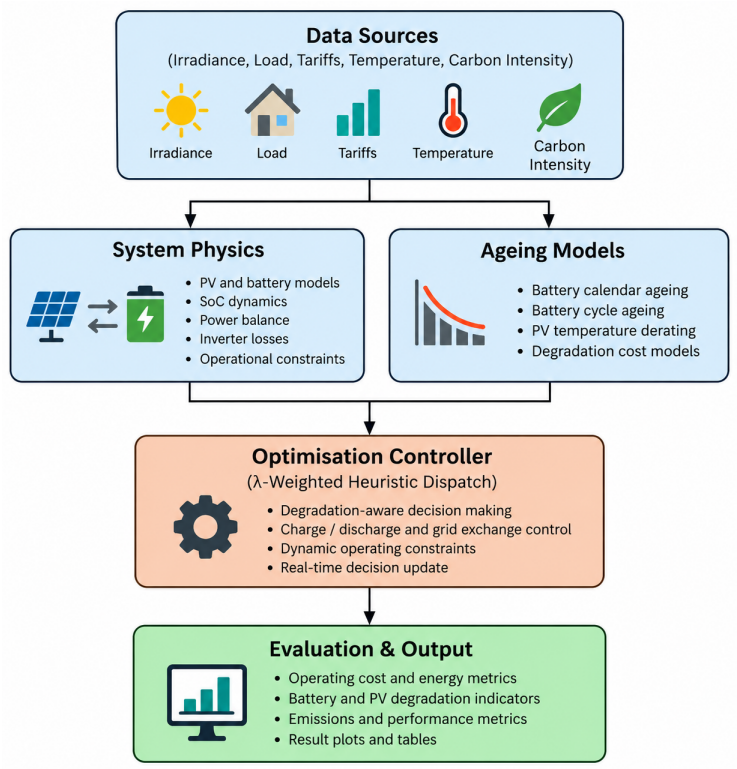


Figure 2. Architecture of the degradation-aware supervisory dispatch framework integrating system dynamics, ageing models, inverter interfaces, and operational decision logic.

3.1. System Model

The energy system comprises a photovoltaic (PV) array, a battery energy storage system (BESS), and a grid connection supplying residual demand and receiving surplus generation. At each control interval, the system model evaluates the AC-side power balance, accounting for PV generation, battery charging and discharging, and grid exchanges.

$$P_{\mathrm{pv,ac}}(t) + P_{\mathrm{grid}}^{\mathrm{imp}}(t) + P_{\mathrm{dis}}(t) = P_{\mathrm{load}}(t) + P_{\mathrm{ch}}(t) + P_{\mathrm{grid}}^{\mathrm{exp}}(t). \quad (1)$$

Here, $P_{\mathrm{pv,ac}}$ denotes the AC power delivered by the PV inverter, P_{ch} and P_{dis} represent AC-side battery charging and discharging powers, and $P_{\mathrm{grid}}^{\mathrm{imp}}$ and $P_{\mathrm{grid}}^{\mathrm{exp}}$ denote grid import and export, respectively.

The battery state of charge is updated using a discrete energy-balance model that incorporates charging, discharging, and inverter conversion efficiencies. This reduced-

order representation is widely adopted in degradation-aware dispatch studies requiring repeated evaluation [77,78].

$$SoC(t+1) = SoC(t) + \frac{\eta_{ch}\eta_{inv,b}P_{ch}(t)\Delta t}{E_{nom}} - \frac{P_{dis}(t)\Delta t}{\eta_{dis}\eta_{inv,b}E_{nom}}. \quad (2)$$

Here, E_{nom} is the nominal battery energy capacity, Δt is the control interval, and η_{ch}, η_{dis}, and $\eta_{inv,b}$ denote charging, discharging, and battery inverter efficiencies, respectively. Power is expressed in kW, energy in kWh, and Δt in hours.

Battery operational limits are enforced through the state-of-charge and power constraints. These restrictions prevent operation outside the configured battery limits, while the dispatch controller accounts for the available charging and discharging headroom.

$$SoC_{\min} \le SoC(t) \le SoC_{\max}, \quad (3)$$

$$0 \le P_{ch}(t) \le P_{ch}^{\max}, \qquad 0 \le P_{dis}(t) \le P_{dis}^{\max}. \quad (4)$$

Together, (1)–(4) provide a compact representation of the operational physics of the hybrid PV–battery system for integration with the supervisory dispatch framework.

3.2. Inverter-Interfaced Power Conversion

The photovoltaic array and battery energy storage system are interfaced with the AC network through separate power electronic conversion stages. The supervisory dispatch layer determines the active-power references supplied to these resources at each control interval, accounting for inverter conversion efficiencies and rated capacities.

For the photovoltaic interface, the available AC-side power is

$$P_{pv,ac}(t) = \min\left\{\eta_{inv,pv}P_{pv,temp}(t), P_{inv,pv}^{rated}\right\}, \quad (5)$$

where $P_{pv,temp}$ denotes the temperature-corrected PV power after the prescribed ageing adjustment, and $\eta_{inv,pv}$ is the PV inverter efficiency.

For the battery interface, the net AC-side power is

$$P_{batt,ac}(t) = P_{dis}(t) - P_{ch}(t). \quad (6)$$

Here, P_{ch} and P_{dis} are the AC-side charging and discharging powers. The corresponding DC-side powers are $\eta_{inv,b}P_{ch}(t)$ and $P_{dis}(t)/\eta_{inv,b}$, respectively, where $\eta_{inv,b}$ is the battery inverter efficiency. These conversion relationships are incorporated into the battery state-of-charge dynamics.

The inverter power references are bounded by their rated active-power capacities,

$$0 \le P_{pv,ac}(t) \le P_{inv,pv}^{rated}, \qquad |P_{batt,ac}(t)| \le P_{inv,b}^{rated}. \quad (7)$$

This representation retains the energy-management focus of the study while accounting for inverter conversion losses and active-power limits without modelling converter switching dynamics.

3.3. Battery Degradation Model

Battery ageing is represented using complementary calendar and cycle degradation components. This reduced-order formulation balances physical interpretability with com-

putational efficiency and is consistent with recent degradation-aware energy management approaches [78–80].

The following reduced-order expressions adopt established calendar- and cycle-ageing principles, with simplified functional forms and illustrative coefficients selected for comparative simulation [44,78,80]. Calendar ageing represents capacity loss associated with time, temperature, and state of charge. It is evaluated using a semi-empirical Arrhenius-type approximation,

$$\Delta Q_{cal}(t) = k_{cal} \exp\left(-\frac{E_a/R}{T_b(t)}\right)\left[0.5 + 0.5SoC_{avg}(t)\right]\Delta t, \tag{8}$$

where k_{cal} is the calendar ageing coefficient, E_a/R is the activation-energy-to-gas-constant ratio, T_b is the battery temperature in kelvin, and SoC_{avg} is the average state of charge over the evaluated interval.

Cycle ageing is estimated from incremental variations in the state-of-charge trajectory using a power-law approximation,

$$\Delta Q_{cyc} = \sum_{i=1}^{N_{\Delta SoC}} k_{cyc}|\Delta SoC_i|^{\alpha}, \tag{9}$$

where k_{cyc} is the cycling coefficient, α is the cycle-wear exponent, and $N_{\Delta SoC}$ denotes the number of evaluated SoC increments. This approximation represents cycling-related wear without requiring detailed electrochemical modelling or rainflow cycle counting.

The combined capacity loss is converted into an economic proxy based on the assumed battery replacement value,

$$C_{deg,batt} = \frac{C_{replacement}}{Q_{nom}}\left(\sum_t \Delta Q_{cal}(t) + \Delta Q_{cyc}\right), \tag{10}$$

where $C_{replacement}$ is the assumed battery replacement cost and Q_{nom} is the illustrative capacity-loss normalisation reference. Calendar and cycle losses are expressed in ampere-hours under the adopted parameterisation.

For operational dispatch, battery degradation is represented by a prescribed marginal penalty rather than directly converting the estimated capacity loss into a time-varying electricity price. The effective penalty is

$$\tilde{\pi}_{deg,batt}(t) = \lambda_b(t)\pi_{deg,batt}, \tag{11}$$

where, $\pi_{deg,batt}$ denotes the prescribed marginal battery-wear penalty in GBP/kWh, while $\lambda_b(t)$ determines its contribution to the discharge decision. This penalty is distinct from the degradation cost calculated in Equation (10). The latter provides a comparative estimate of model-derived capacity loss, whereas the prescribed marginal penalty modifies the effective discharge price only when the corresponding battery degradation weight is nonzero. Consequently, reductions in battery cycling may also arise from policy-specific SoC limits and charging or discharging thresholds, independently of degradation-cost weighting.

The ageing parameters used in the implementation are $k_{cal} = 1.2 \times 10^{-5}$ Ah/h, $E_a/R = 4000$ K, $k_{cyc} = 2.5 \times 10^{-4}$ Ah, and $\alpha = 1.5$ (dimensionless), with state of charge represented as a fraction and time expressed in hours. These coefficient units follow from the dimensional conventions of the implemented reduced-order equations.

The nominal battery energy capacity is $E_{nom} = 5.0$ kWh. The assumed replacement cost is GBP 3500, and $Q_{nom} = 1000$ Ah is an illustrative capacity-loss normalisation reference rather than a charge capacity derived from the configured battery energy and

voltage. The ageing coefficients are study-specific assumptions informed by established calendar- and cycle-ageing principles [44,78,80], not experimentally calibrated parameters for a specified battery chemistry.

Accordingly, the reported capacity-fade percentages and degradation-cost estimates are comparative model-derived indicators. They should not be interpreted as physically calibrated battery state-of-health changes, validated service-life predictions, or replacement-cost forecasts.

3.4. PV Degradation Model

PV performance loss is represented through long-term material degradation and short-term temperature-induced derating. Long-term degradation is approximated using a linear reduction in available power over time, consistent with simplified PV performance assessments [19,20]. The degraded PV power is expressed as

$$P_{pv,deg}(t) = P_{pv}(t)\left(1 - \gamma \frac{t}{t_{year}}\right), \tag{12}$$

where γ is the assumed annual degradation rate and t_{year} denotes one year in the same time units as t.

Short-term thermal effects are represented using a first-order temperature correction, consistent with conventional PV performance modelling [18,19]. The temperature-adjusted PV power is

$$P_{pv,temp}(t) = P_{pv,deg}(t)\Big[1 - \beta(T_{cell}(t) - T_{ref})\Big], \tag{13}$$

where β is the PV temperature coefficient, T_{cell} is the cell temperature, and T_{ref} is the reference temperature.

The resulting PV power is converted to AC-side power through (5) before entering the system power balance. The economic impact of PV performance loss is estimated using the difference between the reference and temperature-corrected power, valued at the prevailing electricity import tariff.

$$C_{loss,pv}(t) = \big[P_{pv}(t) - P_{pv,temp}(t)\big]\,\pi_{value}(t)\Delta t, \tag{14}$$

Here, $\pi_{value}(t)$ represents the electricity import tariff in GBP/kWh, and Δt is the simulation interval in hours. The expression provides a signed operational valuation of the difference between reference PV power and modelled available PV power. Positive values indicate a reduction relative to the reference, while negative values may arise when favourable cell temperatures increase PV output above the reference level. Accordingly, $C_{loss,pv}(t)$ is interpreted as a modelled PV performance-cost indicator rather than a nonnegative measure of irreversible material degradation or a directly incurred electricity cost.

PV performance is additionally summarised using a modelled relative-power indicator for intervals with nonzero reference PV power. This indicator compares temperature-adjusted PV power with the reference PV power and is not intended to represent the standardised system-level PV performance ratio.

$$PR(t) = \frac{P_{pv,temp}(t)}{P_{pv}(t)} \times 100\%, \tag{15}$$

The PV degradation trajectory is prescribed independently of battery dispatch. Its influence is reflected in available PV generation and performance evaluation, rather than through active control of the underlying PV ageing process.

3.5. Degradation-Aware Dispatch Framework

The proposed energy-management framework evaluates operational decisions in terms of electricity cost and degradation-related performance. Rather than solving a multi-objective optimisation problem at each control interval, a structured heuristic is adopted to incorporate battery degradation awareness into deterministic dispatch decisions. This approach avoids the computational requirements of repeated mathematical optimisation while retaining explicit control over battery operating constraints [43,77,81].

The net electricity cost over the evaluation horizon H is calculated from grid imports and exports,

$$J_{energy} = \sum_{t \in H} \left[\pi_{imp}(t) P_{grid}^{imp}(t) - \pi_{exp}(t) P_{grid}^{exp}(t) \right] \Delta t, \tag{16}$$

where π_{imp} and π_{exp} denote the import and export tariffs, respectively. This expression provides the economic evaluation metric and is not directly minimised using a numerical optimisation solver.

Battery degradation awareness is incorporated into the dispatch decision through an effective electricity price,

$$\pi_{eff}(t) = \pi_{imp}(t) - \lambda_b(t) \pi_{deg,batt}, \tag{17}$$

where $\lambda_b(t)$ is the applicable degradation weighting factor and $\pi_{deg,batt}$ is the prescribed marginal battery-wear penalty. Increasing the degradation weight reduces the effective value of battery discharge, making discharge less attractive unless the prevailing tariff is sufficiently high.

The controller evaluates this adjusted price against the configured discharge threshold, subject to available PV generation, load demand, battery state of charge, and inverter power limits. The adaptive supervisory layer further adjusts the degradation weight and discharge threshold according to operating conditions, as described in the following subsection.

The PV-loss weighting coefficient, λ_{pv}, is retained for performance assessment and does not directly modify battery dispatch or the prescribed PV ageing trajectory. The controller therefore represents a deterministic, degradation-informed dispatch heuristic rather than a numerical multi-objective optimisation solver.

3.6. Adaptive Supervisory Control

To extend the fixed-weight degradation-aware dispatch, a lightweight supervisory layer adjusts the battery degradation penalty according to the prevailing operating conditions. At each control interval, a bounded stress score, $S_b(t)$, is evaluated from the battery state of charge, cell temperature, load demand, and electricity import tariff. The adaptive battery weight is then updated as

$$\lambda_b(t) = \lambda_{b,\min} + S_b(t)(\lambda_{b,\max} - \lambda_{b,\min}), \tag{18}$$

where $\lambda_{b,\min} = 0$ and $\lambda_{b,\max} = 0.8$ are the configured weighting limits.

The temperature indicator S_T is derived from modelled PV cell temperature rather than measured battery temperature. It is therefore used as a prescribed thermal supervisory signal. The battery stress score is calculated as

$$S_b(t) = \text{clip}_{[0,1]}[0.45 S_{SoC}(t) + 0.35 S_T(t) + 0.10 S_L(t) + 0.10 S_\pi(t)], \tag{19}$$

where S_{SoC}, S_T, S_L, and S_π denote the normalised SoC, thermal, load, and tariff stress indicators, respectively.

For compact representation, define the bounded ramp function

$$r(x;a,b) = \mathrm{clip}_{[0,1]}\left(\frac{x-a}{b-a}\right), \qquad b > a, \tag{20}$$

where $\mathrm{clip}_{[0,1]}(x) = \min\{1, \max\{0, x\}\}$. The individual stress indicators are

$$\begin{aligned} s_n(t) &= \mathrm{clip}_{[0,1]}\left(\frac{SoC(t) - SoC_{\min}}{SoC_{\max} - SoC_{\min}}\right), \\ S_{SoC}(t) &= \max\{1 - r(s_n(t); 0.15, 0.40), r(s_n(t); 0.60, 0.85)\}, \\ S_T(t) &= r(T_{cell}(t); 30, 40), \\ S_L(t) &= \mathrm{clip}_{[0,1]}\left(\frac{P_{load}(t)}{3.0}\right), \\ S_\pi(t) &= r(\pi_{imp}(t); 0.19, 0.33). \end{aligned} \tag{21}$$

Temperature is expressed in degrees Celsius, load in kW, and electricity price in GBP/kWh. The SoC indicator increases near its operating limits, while the other indicators increase with their respective inputs. Since S_T uses modelled PV cell temperature, it is an operational supervisory proxy rather than a direct measure of battery thermal ageing.

A separate thermal protection mechanism adjusts the discharge price threshold according to

$$\pi^{eff}_{high}(t) = \pi_{high} + k_T S_T(t), \tag{22}$$

where $\pi_{high} = 0.31$ GBP/kWh and $k_T = 0.02$ GBP/kWh. The lower charging-price threshold is fixed at 0.25 GBP/kWh. The effective degradation penalty and thermal threshold are supplied to the deterministic dispatch controller without changing its physical constraints.

The supervisor also evaluates a PV-related weighting signal,

$$\begin{aligned} S_{pv}(t) &= \mathrm{clip}_{[0,1]}\left[0.65 S_T(t) + 0.35\,\mathrm{clip}_{[0,1]}\left(\frac{P_{pv,temp}(t)}{3.6}\right)\right], \\ \lambda_{pv}(t) &= 0.20 S_{pv}(t). \end{aligned} \tag{23}$$

This signal is retained for supervisory monitoring and degradation-related assessment. It does not directly alter battery dispatch or the prescribed PV ageing trajectory. The resulting supervisory structure therefore provides state-dependent battery protection through transparent, bounded rules while preserving the computational simplicity of the underlying dispatch controller.

Controller Algorithm

Algorithm 1 summarises the deterministic dispatch procedure executed at each 15 min interval. The controller prioritises local PV utilisation and surplus charging, with battery discharge and grid charging governed by tariff thresholds and operating constraints. Scenario-specific SoC limits and thresholds are applied before dispatch. The Baseline favours grid charging during 00:00–06:59 and discharge during 16:00–22:59; the Battery+PV-Aware policy inhibits discharge at $T_{cell} \geq 35\,^\circ$C. The Adaptive-Supervisory policy updates its degradation weight and discharge threshold according to operating conditions.

The 35 °C PV-cell-temperature threshold is an illustrative supervisory setting used to test conservative discharge behaviour under elevated PV operating temperatures. It is not derived from battery thermal limits or experimental PV ageing measurements. The

restriction therefore represents a prescribed operating policy, not active control of PV material degradation or a calibrated battery-protection mechanism.

Algorithm 1 Degradation-Aware Dispatch Logic.

Inputs: SoC, $P_{pv,ac}$, P_{load}, π_{imp}, T_{cell}, scenario s
Outputs: P_{ch}, P_{dis}, P_{grid}^{imp}, P_{grid}^{exp}
Load scenario-specific SoC limits, tariff thresholds, and λ_b
Apply adaptive supervisory updates or Baseline time-of-use overrides, as applicable
$\pi_{eff} \leftarrow \pi_{imp} - \lambda_b \pi_{deg,batt}$
$D \leftarrow P_{load} - P_{pv,ac}$
Determine available charging and discharging power
if $s =$ Battery+PV-Aware **and** $T_{cell} \geq 35\,^{\circ}\mathrm{C}$ **then**
    Disable battery discharge
end if
if $D > 0$ **then**
    if $\pi_{eff} > \pi_{high}^{use}$ **and** discharge is available **then**
        Discharge battery; import remaining demand
    else if $\pi_{imp} < \pi_{low}^{use}$ **and** charging is available **then**
        Charge battery from grid; import required power
    else
        Import net demand from grid
    end if
else
    Charge battery from PV surplus; export remainder
end if
Enforce operating limits and update SoC using (2)

Available battery power accounts for the scenario-specific SoC window, battery and inverter ratings, and remaining energy capacity. Conversion efficiencies are included in the SoC update. The controller implements deterministic operating rules rather than numerical optimisation.

4. Experimental Design

Simulation experiments evaluate electricity operating cost, battery cycling, modelled capacity fade, and PV performance. The experimental setup follows recent degradation-aware energy management studies that assess operational trade-offs under consistent physical and economic conditions [67,72,77,78]. A full-year simulation horizon with 15 min resolution is adopted to capture seasonal demand variability, thermal effects, and cumulative battery operation.

4.1. Dataset Preparation

The primary analysis uses reproducible synthetic operational profiles representing residential electricity demand, solar irradiance, ambient temperature, and tariff-driven dispatch conditions. Irradiance and temperature are generated from parameterised seasonal and daily patterns, while residential demand combines time-dependent consumption patterns with stochastic variability. Representative electricity import and export tariffs are included to evaluate operating costs under different dispatch conditions [77,82].

The dataset is generated using the procedures, parameters, and random seeds specified in the accompanying repository. Identical input profiles are applied to all four principal dispatch scenarios to ensure consistent comparison. Supplementary tariff sensitivity experiments modify only the import-price profile, retaining the remaining system inputs and model parameters.

4.2. Validation Using Measured Residential Load and Meteorological Data

To assess the robustness of the proposed degradation-aware dispatch beyond the synthetic operating profiles, a supplementary evaluation is performed using recorded residential electricity demand and historical meteorological inputs. The objective is to examine whether the degradation–cost trade-offs observed in the full-year simulation persist under externally sourced operating conditions [72,77,83].

Household electricity demand is obtained from the open-access UK-DALE dataset. Solar irradiance and ambient temperature are sourced from the European Commission Joint Research Centre's Photovoltaic Geographical Information System (PVGIS) [84]. The PVGIS data are used to estimate PV generation through the system's prescribed power and temperature models; PV electricity production is therefore model-derived rather than directly measured. An approximate Oxford-area meteorological reference is adopted for this evaluation.

The datasets are aligned to a common 15 min time base. Missing residential demand observations are excluded, and the longest continuous period is selected to avoid introducing artificial transitions into the battery state trajectory. The resulting validation dataset comprises 19,032 consecutive intervals, covering 11 April to 26 October 2013 (198.25 days).

The same nominal system parameters, degradation models, and four dispatch policies used in the primary simulation are retained without recalibration. Battery energy throughput, equivalent full cycles, and net grid electricity cost are evaluated over the actual observation period and compared against the baseline policy. This supplementary evaluation tests the consistency of simulated dispatch behaviour under externally sourced inputs, rather than providing physical or hardware-in-the-loop validation of the PV–battery system.

4.3. Experimental Scenarios

Four operational scenarios are evaluated using identical demand, PV generation, tariff profiles, and nominal system parameters, with policy-specific dispatch thresholds, battery operating windows, and degradation-related settings:

- Baseline: A cost-oriented reference policy with $\lambda_b = \lambda_{pv} = 0$. It uses the nominal SoC operating range of 10–90%, price thresholds of 0.19 and 0.33 GBP/kWh, and time-of-use charging and discharging preferences.
- Battery-Aware: A battery-conservative policy that narrows the SoC operating range to 15–85% and uses charging and discharging price thresholds of 0.25 and 0.31 GBP/kWh, respectively. The implemented configuration retains $\lambda_b = 0$; consequently, battery protection is achieved through the modified operating policy rather than an explicit marginal degradation penalty.
- Battery+PV-Aware: A fixed degradation-aware policy employing a narrower SoC range of 20–80%, charging and discharging thresholds of 0.26 and 0.325 GBP/kWh, and a battery degradation weight of $\lambda_b = 1.2$. A PV-loss weight of $\lambda_{pv} = 0.20$ is retained for performance assessment, while PV ageing remains exogenous to dispatch. Battery discharge is additionally restricted at cell temperatures of 35 °C or above.
- Adaptive-Supervisory: A state-dependent policy in which the battery degradation weight and discharge threshold are adjusted using the supervisory stress indicators described previously. The policy retains deterministic dispatch logic and enforces its configured battery operating limits.

These scenarios compare complete operating policies rather than isolate degradation weighting. In particular, the Battery-Aware policy has no active marginal degradation penalty; its cycling reduction arises from modified SoC limits and tariff thresholds. Differences among the four policies therefore reflect their combined operating constraints and

supervisory settings. The separate adaptive ablations isolate the incremental contribution of the two supervisory mechanisms.

To distinguish the contribution of supervisory adaptation from these policy-level differences, additional controlled ablation experiments evaluate the adaptive battery-weight and thermal-protection mechanisms under the original tariff and two supplementary synthetic tariff profiles.

4.4. Performance Evaluation

System performance is evaluated using electricity operating cost, battery energy throughput, equivalent full cycles (EFCs), modelled capacity fade, degradation-related cost, PV relative-power indicators, and computational performance. These metrics support comparative assessment of operational and degradation-related trade-offs [78,81,85].

Net electricity cost is calculated from grid import expenditure less export revenue, as defined in (16). Battery energy throughput is reported as cumulative discharged energy, and the equivalent full cycles are calculated as

$$EFC = \frac{\sum_{t \in H} P_{dis}(t)\Delta t}{E_{nom}}, \tag{24}$$

where E_{nom} is the nominal battery energy capacity. Battery capacity fade and its associated economic proxy are estimated using the calendar and cycle degradation models described previously. These estimates provide relative indicators of modelled degradation and are not interpreted as experimentally calibrated predictions of battery service life.

PV performance is evaluated using the temperature- and ageing-adjusted power model. The reported degradation indicators are model-derived and are not interpreted as experimentally validated lifetime estimates.

For the primary 365-day experiment, cumulative metrics are reported as annual totals. The supplementary UK-DALE/PVGIS evaluation reports totals over its actual 198.25-day observation period without annualisation. Policy comparisons are expressed as absolute values and percentage changes relative to the corresponding baseline under identical input conditions.

All policy comparisons are deterministic and use matched input profiles. Cost and cycling differences are reported descriptively, with no inferential confidence intervals or statistical significance claims.

5. Results

The degradation-aware dispatch framework was evaluated over a full year at 15 min resolution, comprising 35,040 operating intervals. This enabled the assessment of economic, operational, and degradation-related performance under consistent input conditions. The primary results compare four simulated dispatch policies, while supplementary experiments examine adaptive supervisory behaviour under alternative tariff profiles.

5.1. Economic Performance

Economic performance is assessed through the annual net electricity operating cost, calculated from grid import expenditure less export revenue using (16). Table 2 summarises the results for the four dispatch policies.

The Baseline records an annual operating cost of GBP 1076.27. The Battery-Aware policy reduces this to GBP 1075.13, representing a marginal saving of 0.11%. In contrast, the Battery+PV-Aware policy increases the annual cost to GBP 1096.49, or 1.88% above the Baseline. The Adaptive-Supervisory policy records the lowest cost of GBP 1056.74, corresponding to a reduction of 1.81%.

Table 2. Annual electricity operating cost and battery cycling performance across the four dispatch policies.

Scenario	Cost (GBP)	Cost Change (%)	EFCs	EFC Reduction (%)
Baseline	1076.27	–	281.59	–
Battery-Aware	1075.13	−0.11	230.81	18.03
Battery+PV-Aware	1096.49	+1.88	199.66	29.10
Adaptive-Supervisory	1056.74	−1.81	257.68	8.49

These results demonstrate that more conservative battery operation does not necessarily produce a substantial economic penalty. However, the differences reflect the combined effects of policy-specific SoC limits, charging and discharging thresholds, and applicable degradation penalties. They should therefore not be attributed exclusively to degradation weighting or interpreted as evidence of globally optimal dispatch.

The relatively small cost differences are considered alongside battery cycling and degradation indicators in the following subsections to establish the corresponding operational trade-offs.

5.2. Lifecycle Performance

Lifecycle performance is characterised using battery energy throughput, equivalent full cycles (EFCs), and estimated state-of-health loss derived from the degradation models. The percentage capacity loss is calculated as

$$\Delta SoH = \frac{\sum_{t=1}^{T} \Delta Q_{cal}(t) + \Delta Q_{cyc}}{Q_{nom}} \times 100\%, \tag{25}$$

where Q_{nom} denotes the illustrative capacity-loss normalisation reference defined in Section 3.3, and ΔQ_{cal} and ΔQ_{cyc} represent the modelled calendar and cycling-related capacity losses, respectively.

The annual cycling results are summarised in Table 2. The Baseline completes 281.59 EFCs, compared with 230.81 EFCs for Battery-Aware and 199.66 EFCs for Battery+PV-Aware. These correspond to reductions of 18.03% and 29.10%, respectively. The Adaptive-Supervisory policy completes 257.68 EFCs, representing an 8.49% reduction relative to the Baseline.

The Battery+PV-Aware policy therefore provides the greatest reduction in cycling intensity, although this is accompanied by a modest increase in electricity operating cost. In contrast, the Adaptive-Supervisory policy achieves a smaller cycling reduction while maintaining the lowest annual electricity cost. These differences illustrate the trade-off between conservative battery utilisation and short-term economic performance.

The estimated degradation indicators decrease under the more restrictive battery operating policies, consistent with their lower cycling throughput. However, the reduced-order ageing model provides comparative degradation estimates rather than experimentally calibrated predictions of battery lifetime. Consequently, the observed EFC reductions should not be interpreted as proportional extensions of battery service life or direct evidence of reduced replacement frequency.

5.3. Modelled Battery Capacity Fade

Table 3 compares the modelled battery capacity fade across the four dispatch policies using the illustrative ageing parameters described in Section 3.3.

Table 3. Modelled battery capacity fade under the four dispatch policies.

Scenario	Capacity Fade (%)
Baseline	0.00519
Battery-Aware	0.00433
Battery+PV-Aware	0.00365
Adaptive-Supervisory	0.00478

The modelled capacity fade decreases from 0.00519% for the Baseline to 0.00365% for Battery+PV-Aware. These illustrative estimates indicate relative degradation differences, but are not experimentally calibrated predictions of battery lifetime.

5.4. Computational Performance

The computational requirements of the four dispatch policies are assessed using the average software execution time per simulation interval. The controller performs deterministic power allocation and bounded supervisory calculations without solving a horizon-wide mathematical optimisation problem. Table 4 summarises the computational results alongside the annual inverter conversion losses.

Table 4. Computational performance and annual battery inverter losses.

Scenario	Runtime (ms/Step)	Battery Loss (kWh)
Baseline	0.258	126.28
Battery-Aware	0.261	103.66
Battery+PV-Aware	0.256	89.67
Adaptive-Supervisory	0.288	115.73

Average software execution time ranges from 0.256 to 0.288 ms per simulated interval. The annual PV inverter losses remain constant at 65.22 kWh, while battery inverter losses vary with battery utilisation. The reported runtime excludes data acquisition, communication, and actuation delays and does not establish hardware real-time performance.

5.5. Dispatch Behaviour

Figure 3 illustrates a representative seven-day operational profile under the Battery+PV-Aware policy. The simulated trajectories show the interaction between PV generation, residential demand, battery charging and discharging, grid exchange, and state of charge. Battery operation follows the configured charging and discharging thresholds while remaining within the prescribed SoC and power limits.

The Battery+PV-Aware policy applies a narrower battery operating window and more conservative discharge conditions than the Baseline. These restrictions limit battery utilisation and contribute to the lower cumulative cycling reported in the annual results. The observed behaviour reflects the combined effect of the operating thresholds, SoC constraints, thermal restrictions, and degradation-related settings rather than any single control parameter.

Although PV availability influences the energy balance and charging opportunities, the underlying PV ageing trajectory remains prescribed independently of dispatch. Consequently, the observed reduction in battery cycling should not be interpreted as evidence of active PV degradation control.

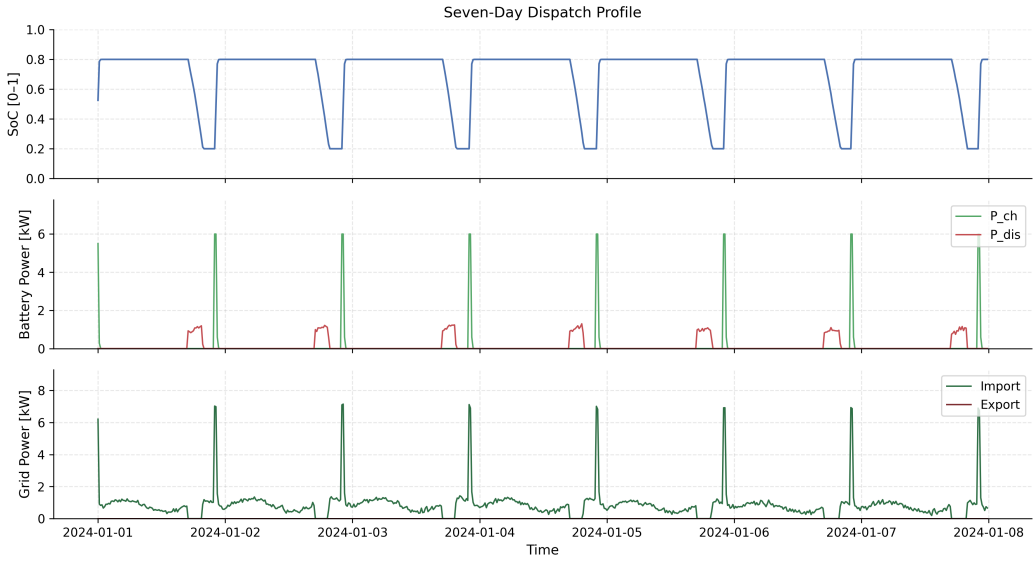


Figure 3. Representative seven-day dispatch profile under the Battery+PV-Aware policy.

5.6. Statistical Interpretation

The four policies are evaluated using matched demand, PV generation, and tariff inputs, allowing direct comparison under the specified simulation conditions. The annual differences in electricity cost relative to the Baseline are −0.11%, +1.88%, and −1.81% for Battery-Aware, Battery+PV-Aware, and Adaptive-Supervisory dispatch, respectively.

These are results from deterministic scenarios. No inferential test or confidence interval is reported. Statistical significance and generalisation to other operating conditions are not established. The observed EFC reductions similarly describe the evaluated trajectories rather than the uncertainty in different weather years, households, or tariffs.

5.7. Adaptive Supervisory Control Performance

The Adaptive-Supervisory policy was evaluated over the same full-year, 15 min horizon as the fixed policies. As reported in the preceding comparisons, it achieves the lowest annual electricity cost (GBP 1056.74), reducing cost by 1.81% and equivalent full cycles (EFCs) by 8.49% relative to the Baseline. However, its cycling reduction is smaller than those of the fixed Battery-Aware and Battery+PV-Aware policies, indicating a different cost–degradation trade-off.

Controlled ablations were conducted to distinguish the effects of adaptive battery-weight adjustment and thermal discharge protection from the underlying dispatch configuration. Under the original three-level tariff, disabling either or both mechanisms produced identical dispatch trajectories, costs, and EFCs. Thus, the observed improvements relative to the Baseline cannot be attributed to active supervisory adaptation under this tariff.

Table 5 evaluates the contribution of the adaptive supervisory mechanisms by comparing the controller with adaptive degradation weighting and thermal discharge protection jointly enabled and disabled under three electricity import-price profiles. The reference time-of-use (TOU) tariff corresponds to the main annual simulation, while the smoothed TOU and variable synthetic tariffs provide supplementary sensitivity tests. The smoothed TOU tariff reduces short-term price fluctuations, whereas the variable synthetic tariff introduces an independently generated periodic price pattern. Both supplementary profiles are prescribed synthetic sensitivity inputs, with all other system inputs and parameters held constant. Annual electricity cost and battery equivalent full cycles (EFCs) are compared to assess the economic and cycling effects of the supervisory mechanisms.

Table 5. Combined supervisory ablation under three tariff profiles.

	Enabled		Disabled	
Tariff	**Cost (GBP)**	**EFCs**	**Cost (GBP)**	**EFCs**
Reference TOU	1056.74	257.68	1056.74	257.68
Smoothed TOU	1086.74	255.24	1087.81	260.83
Variable synthetic	1609.88	142.22	1610.68	158.29

For the reference TOU tariff, import prices take values of 0.09, 0.21, and 0.39 GBP/kWh. With a base discharge threshold of 0.31 GBP/kWh and a maximum weighted degradation penalty of 0.024 GBP/kWh, none of these prices falls within the weight-sensitive discharge range. Consequently, varying the battery weight does not change the price-based discharge decision under this tariff.

Relative to the disabled-supervisor configuration, adaptive supervision reduces EFCs by 2.14% and 10.15% under the smoothed and independent tariffs, respectively, with corresponding cost reductions of approximately 0.10% and 0.05%. Battery-weight adaptation influences both supplementary cases, whereas thermal protection affects dispatch only under the independent tariff.

These findings indicate that adaptive supervision provides incremental cost–cycling benefits only when tariff conditions activate its supervisory mechanisms. Under the original tariff, no additional benefit is observed. The fixed Battery+PV-Aware policy achieves greater cycling reduction under the main annual conditions, but at a higher electricity cost.

To isolate the degradation weighting from the combined supervisory mechanisms, Table 6 compares zero, fixed, and adaptive battery weights under identical operating constraints across the same three tariff profiles.

Table 6. Fixed and adaptive degradation weighting under identical operating constraints.

	Reference TOU		Smoothed TOU		Variable Synthetic	
Weighting	**Cost (GBP)**	**EFCs**	**Cost (GBP)**	**EFCs**	**Cost (GBP)**	**EFCs**
Zero	1056.74	257.68	1087.81	260.83	1610.75	157.95
Fixed 0.4	1056.74	257.68	1087.74	259.90	1608.89	146.54
Fixed 0.8	1056.74	257.68	1087.13	254.13	1621.79	92.40
Adaptive	1056.74	257.68	1086.74	255.24	1609.88	142.22

Under the reference TOU tariff, all weighting configurations produce identical outcomes because import prices remain outside the weight-sensitive discharge threshold range. Under supplementary tariffs, weighting influences dispatch and reveals distinct cost–cycling trade-offs. Adaptive weighting achieves the lowest cost under smoothed TOU, but does not consistently outperform fixed weighting under the variable synthetic tariff.

5.8. Supplementary Results Using Measured Data

The four dispatch policies were further evaluated using UK-DALE residential demand and PVGIS-derived meteorological inputs, retaining the same system parameters, degradation models, and dispatch logic. The dataset comprises 19,032 consecutive 15 min intervals (198.25 days, 11 April–26 October 2013). Results are reported over this period without annualisation.

As shown in Table 7, all three alternative policies reduce battery cycling relative to the Baseline. Battery+PV-Aware achieves the largest reduction (20.67%). This preserves the qualitative trend observed in the annual synthetic simulation, although the reduction magnitudes differ with operating inputs. Negative net electricity costs indicate that modelled

export revenue exceeds import expenditure under the assumed tariffs. The absolute cost differences remain small, and their statistical significance has not been established.

Table 7. Dispatch performance using UK-DALE demand and PVGIS meteorological inputs over 198.25 days.

Scenario	Net Cost (GBP)	EFCs	EFC Reduction (%)
Baseline	−7.69	73.81	–
Battery-Aware	−9.89	59.40	19.52
Battery+PV-Aware	−9.36	58.55	20.67
Adaptive-Supervisory	−9.93	59.59	19.27

These results support the consistency of comparative cycling trends across synthetic and externally sourced inputs. However, PV generation remains model-derived, tariffs are prescribed, and degradation is not physically measured. The experiment therefore provides measured-input simulation evidence rather than physical validation of battery lifetime or a synchronised digital twin.

6. Discussion

The proposed framework demonstrates how degradation-related indicators can inform PV–battery dispatch through transparent, computationally lightweight operating rules. Compared with the Baseline, the Battery-Aware and Battery+PV-Aware policies reduce annual equivalent full cycles (EFCs) by 18.03% and 29.10%, respectively, with changes in electricity-cost of −0.11% and +1.88%. These results reflect combined differences in SoC limits, tariff thresholds, thermal restrictions, and degradation weighting rather than the isolated effect of any single mechanism. Modelled battery capacity fade decreases from 0.00519% to 0.00365% between the Baseline and Battery+PV-Aware policies. However, the illustrative ageing parameters do not support direct claims about extended service life.

The Adaptive-Supervisory policy achieves annual reductions of 1.81% in operating cost and 8.49% in EFCs relative to the Baseline. Although fixed Battery+PV-Aware dispatch achieves greater cycling reduction, adaptive supervision permits state-dependent adjustment of battery-wear weighting and discharge thresholds. Controlled ablations do not show an incremental supervisory effect under the original three-level tariff, whereas the smoothed and independent synthetic tariffs yield additional EFC reductions of 2.14% and 10.15%, respectively, relative to disabled-supervisor configurations. Thus, supervisory effectiveness depends on tariff structure and threshold interactions rather than dynamic weighting alone.

Supplementary simulations using UK-DALE demand and PVGIS meteorological inputs show the same direction of cycling reduction over 198.25 days. Relative to the Baseline, EFCs decrease by 19.52%, 20.67%, and 19.27% for Battery-Aware, Battery+PV-Aware, and Adaptive-Supervisory dispatch, respectively. Net electricity-cost differences remain small in absolute terms and depend on the assumed tariffs. These findings support comparative consistency across the evaluated inputs but do not constitute physical validation of the degradation models or PV–battery system.

The modelled cycling reductions indicate lower battery utilisation under the evaluated policies, but do not establish longer service life or reduced lifecycle environmental impacts. Quantitative environmental benefits remain unverified.

The modular Python implementation includes a Streamlit dashboard (Figure 4) to examine the dispatch trajectories, degradation indicators, and cost–cycling trade-offs. It provides an interactive simulation-based decision-support environment, rather than a digital twin synchronised with physical equipment.

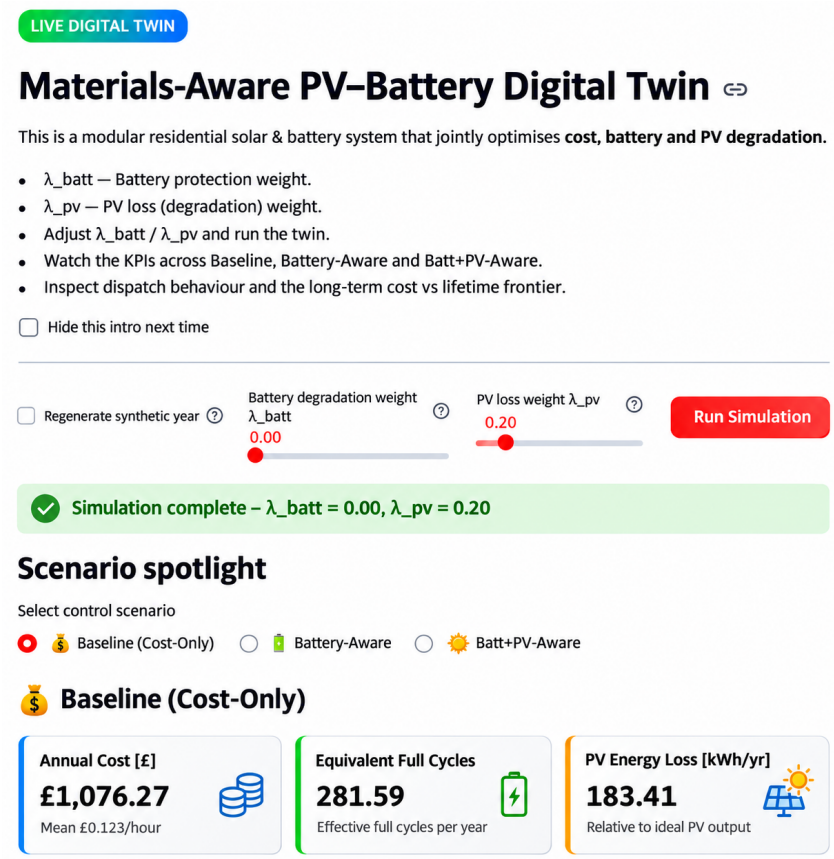


Figure 4. Streamlit interface for examining dispatch, degradation indicators, and operational performance.

Limitations and Future Work

The reduced-order degradation models employed in this study capture selected battery and PV ageing mechanisms but simplify the underlying electrochemical and thermo-mechanical processes. In particular, the battery models do not explicitly represent internal resistance growth, solid–electrolyte interphase evolution, or nonlinear temperature–current interactions. Furthermore, the ageing coefficients are illustrative rather than calibrated against experimental lifetime data. Consequently, the estimated capacity fade and degradation costs are suitable for comparative assessment but cannot establish absolute battery lifetime or replacement intervals. Future research will investigate experimentally calibrated, physics-informed and hybrid degradation models to improve predictive fidelity while retaining computational efficiency.

The principal dispatch policies employ different SoC operating windows, tariff thresholds, and degradation-related settings; their performance differences therefore cannot be attributed exclusively to degradation weighting. A supplementary controlled comparison isolates battery weighting under identical operating constraints and demonstrates that its influence depends on the tariff profile. Under the original three-level tariff, weighting does not alter dispatch, whereas supplementary synthetic tariffs reveal distinct cost–cycling trade-offs between fixed and adaptive weighting. These deterministic findings do not establish general superiority across tariff conditions. Future work will investigate broader parameter sensitivity and comparisons against established optimisation-based controllers. PV ageing remains prescribed independently of dispatch.

The present analysis uses deterministic operating inputs and simulation-based system models. Although supplementary evaluation incorporates measured residential demand and historical meteorological inputs, PV generation remains model-derived. The framework has not undergone physical PV–battery validation, hardware-in-the-loop testing, or

live measurement synchronisation. Economic differences are deterministic outcomes without inferential significance testing. Future work will address uncertainty-aware dispatch, statistical evaluation, lifecycle environmental assessment, and experimental validation.

7. Conclusions

This study developed a degradation-aware, digital-twin-inspired dispatch framework for inverter-interfaced photovoltaic–battery energy systems. The framework integrates reduced-order battery ageing models, prescribed PV degradation, and deterministic energy-management rules to incorporate lifecycle considerations into operational decision-making. The proposed approach provides a computationally lightweight means of examining electricity-cost and battery-preservation trade-offs without requiring numerical optimisation or data-intensive learning methods.

Full-year simulations demonstrate that the Battery-Aware and Battery+PV-Aware policies reduce annual equivalent full cycles by 18.03% and 29.10%, respectively, relative to the Baseline, with corresponding electricity-cost changes of -0.11% and $+1.88\%$. The Adaptive-Supervisory policy achieves an 8.49% reduction in battery cycling alongside a 1.81% reduction in operating cost. These outcomes reflect the combined effects of the respective operating thresholds, battery constraints, and degradation-related settings rather than degradation weighting alone.

The adaptive supervisory extension introduces state-dependent battery degradation weighting and discharge protection. Controlled ablations show no incremental supervisory benefit under the original three-level tariff, but demonstrate cycling reductions of 2.14% and 10.15% under supplementary synthetic tariff profiles. Additional equal-constraints comparisons confirm that degradation weighting influences dispatch under variable tariffs, although adaptive weighting does not consistently outperform fixed alternatives. The resulting cost–cycling trade-offs are therefore conditional on tariff characteristics and controller settings. Average simulation execution time remains below 0.3 ms per interval.

The principal contribution lies in providing a transparent and reproducible framework through which degradation-related indicators can inform routine PV–battery energy management. Battery wear is represented through a marginal dispatch penalty, while PV ageing and temperature-dependent performance losses are incorporated into the system model and evaluation. Supplementary assessment using UK-DALE residential demand and PVGIS meteorological inputs further supports the consistency of battery-cycling reductions, with the three alternative policies achieving reductions of 19.27–20.67% over the 198.25-day observation period.

These findings establish comparative improvements in simulated battery cycling, not experimentally verified lifetime extension or environmental benefits. The ageing parameters remain illustrative, and the present implementation is an offline, simulation-based digital counterpart rather than a physically synchronised digital twin. Future work will prioritise calibrated ageing models, broader operating-condition sensitivity, statistical evaluation, and physical or hardware-in-the-loop validation.

Author Contributions: Conceptualization, A.O., G.A., P.M.U. and G.P.; data curation, A.O.; formal analysis, A.O., G.A., P.M.U. and G.P.; methodology, A.O.; validation, A.O., G.A., P.M.U. and G.P.; visualization, A.O., G.A., P.M.U. and G.P.; software, A.O.; writing—original draft preparation, A.O.; writing—review and editing, G.A., P.M.U. and G.P.; project administration, G.A. and G.P.; supervision, G.A., P.M.U. and G.P. All authors have read and agreed to the published version of the manuscript.

Funding: This research received no external funding.

Data Availability Statement: The complete implementation of the degradation-aware dispatch framework, including source code, configuration files, and simulation output, is available at https://github.com/ogatech4real/Material_Aware_Digital_Twin (accessed on 21 October 2026). An interactive Streamlit-based dashboard is available to visualise dispatch behaviour, degradation metrics, and key performance indicators https://pvbattdt.streamlit.app/ (accessed on 21 October 2026). All simulations are reproducible using fixed random seeds and tested on Python 3.10+. The modular architecture supports reproducibility and extension without modification of the core workflow.

Acknowledgments: The authors acknowledge the support of Teesside University in facilitating this research.

Conflicts of Interest: The authors declare no conflicts of interest.

Abbreviations and Nomenclature

Nomenclature

λ_b, λ_{pv}	Battery degradation and PV loss weights
SoC, SoH, DoD	State of charge, state of health, depth of discharge
S_b	Normalised battery stress indicator
PR	Modelled PV relative-power indicator
$C_{\text{deg},b}$	Estimated battery degradation cost
$C_{\text{loss},pv}$	Modelled PV performance-loss cost
P_{pv}, P_{load}	PV generation and electrical demand
P_{ch}, P_{dis}	Battery charging and discharging power
P_{imp}, P_{exp}	Grid import and export power
Δt	Simulation time-step duration

Abbreviations

PV, BESS	Photovoltaic; battery energy storage system
DT, MPC	Digital twin; model predictive control
AI, DRL	Artificial intelligence; deep reinforcement learning
LID, PID	Light-induced; potential-induced degradation
LCOE, LCOS	Levelised cost of energy; storage
KPI, EFC	Key performance indicator; equivalent full cycle
HIL	Hardware-in-the-loop
DT-M, DT-O	Digital-twin monitoring; operational decision-making
LCO	Lifecycle-related cost modelling

References

1. Singh, P.; Dhundhara, S.; Verma, Y.P.; Tayal, N. Optimal battery utilization for energy management and load scheduling in smart residence under demand response scheme. *Sustain. Energy Grids Netw.* **2021**, *26*, 100432. [CrossRef]
2. Dong, Z.; Tao, Y.; Lai, S.; Wang, T.; Zhang, Z. Powering future advancements and applications of battery energy storage systems across different scales. *Energy Storage Appl.* **2025**, *2*, 1. [CrossRef]
3. Revathi, R.; Senthilnathan, N.; Kumar Chinnaiyan, V. Hybrid optimization approach for power scheduling with PV-battery system in smart grids. *Energy* **2024**, *290*, 130051. [CrossRef]
4. Pillai, G.; Allison, M.; Tun, T.P.; Chandrakumar Jyothi, K.; Kollonoor Babu, E. Facilitating higher photovoltaic penetration in residential distribution networks using demand side management and active voltage control. *Eng. Rep.* **2021**, *3*, e12410. [CrossRef]
5. Odoi-Yorke, F.; Baah, B.; Kissi-Boateng, R.; Opoku, R.; Effah, F.B. Unlocking the potential of redundant energy from solar photovoltaic systems: Navigating global research trends, innovations, and future directions. *Energy Rep.* **2025**, *13*, 6362–6383. [CrossRef]
6. Zhang, J.; Li, J. Revolution in renewables: Integration of green hydrogen for a sus-tainable future. *Energies* **2024**, *17*, 4148. [CrossRef]
7. Ashraf, A.; Sagheer, M. Renewable energy capacity and technological innovations: A review of global trends and future directions. *Environ. Prog. Sustain. Energy* **2025**, *44*, e70071. [CrossRef]
8. Krishna, R.; Vaid, M.; Sinha, M. Trend Analysis of Global Energy Demand, Renewable Energy Production and Potential in India. *Asian J. Environ. Ecol.* **2025**, *24*, 25–38. [CrossRef]

9. Li, X.; Shi, Y.; Zhang, R.; Zhang, X.; Tang, R.; Yang, X.; Lai, J.; Zhang, Y. Research on the integration of mobile energy storage system for enhancing black start capability and resilience in distribution networks under extreme events. *Sustain. Energy Grids Netw.* **2025**, *43*, 101724. [CrossRef]
10. Razmjoo, A.; Ghazanfari, A.; Østergaard, P.A.; Jahangiri, M.; Sumper, A.; Ahmadzadeh, S.; Eslamipoor, R. Moving toward the expansion of energy storage systems in renewable energy systems—A techno-institutional investigation with artificial intelligence consideration. *Sustainability* **2024**, *16*, 9926. [CrossRef]
11. Soussi, A.; Zero, E.; Bozzi, A.; Sacile, R. Enhancing energy systems and rural communities through a system of systems approach: A comprehensive review. *Energies* **2024**, *17*, 4988. [CrossRef]
12. Saranya, S.T.; Bhowmik, P. A comprehensive review of microgrid architectures, power management and re-silient operation. *Energy Rep.* **2026**, *15*, 109021. [CrossRef]
13. Yaldız, A.; Gökçek, T.; Ateş, Y.; Erdinç, O. Overview and advancement of power system topology addressing pre-and post-event strategies under abnormal operating conditions. *Sustain. Energy Grids Netw.* **2024**, *40*, 101562. [CrossRef]
14. Xu, R.; Jiang, Q.; Li, B.; Liu, Y.; Zhu, Y.; Gu, Y.; Liu, T. Frequency-Spectra Impedance Margin Ratio for Stability Analysis of IBR-Penetrated Systems. *IEEE Trans. Power Syst.* **2026**, *41*, 4775–4790. [CrossRef]
15. Kumba, K.; Simon, S.P.; Gundu, V.; Upender, P.; Ra, N.; Sarkar, M. An evaluation of battery degradation and predictive methods under resistive load caused by intermittent solar radiation. *IEEE Access* **2024**, *12*, 33720–33729. [CrossRef]
16. Vasylyev, A.; Vannoni, A.; Sorce, A. Optimal dispatch of Li-Ion battery energy storage, reviewing and con-sidering cycling and calendar ageing models. *Appl. Therm. Eng.* **2025**, *265*, 125597. [CrossRef]
17. Lee, M.; Park, J.; Na, S.I.; Choi, H.S.; Bu, B.S.; Kim, J. An analysis of battery degradation in the integrated energy storage system with solar photovoltaic generation. *Electronics* **2020**, *9*, 701. [CrossRef]
18. Ymer, E.T.; Lemu, H.G.; Tolcha, M.A. Identification of the key material degradation mechanisms affecting silicon solar cells: Systematic literature review. *Results Eng.* **2025**, *27*, 106113. [CrossRef]
19. Chen, K.; Zuo, J.; Chang, R. Compendium of degradation rates of global photo-voltaic (PV) technology: Insights from technology, climate and geography. *Sol. Energy Mater. Sol. Cells* **2025**, *293*, 113839. [CrossRef]
20. IEA PVPS Task 13. Degradation and Failure Modes in New Photovoltaic Cell and Module Technologies, IEA-PVPS Report T13-30:2025. February 2025. Available online: https://iea-pvps.org/key-topics/degradation-failure-modes-new-cell-module-technologies/ (accessed on 13 January 2026).
21. Bonkile, M.P.; Ramadesigan, V. Physics-based models in PV-battery hybrid power systems: Thermal man-agement and degradation analysis. *J. Energy Storage* **2020**, *31*, 101458. [CrossRef]
22. Ruiz, P.L.; Damianakis, N.; Mouli, G.R. Physics-based and data-driven modeling of degradation mechanisms for lithium-ion batteries—A review. *IEEE Access* **2025**, *13*, 21164–21189. [CrossRef]
23. Kumar, V.; Niazi, M.A.; Aslam, U.; Saeed, N.; Aurangzeb, M.; Shah, S.A. A Holistic Optimization Framework for Virtual Power Plants with Physics-Informed Battery Degradation and Probabilistic Stability Constraints. *Future Batter.* **2026**, *9*, 100146. [CrossRef]
24. Semeraro, C.; Olabi, A.G.; Aljaghoub, H.; Alami, A.H.; Al Radi, M.; Dassisti, M.; Abdelkareem, M.A. Digital twin application in energy storage: Trends and challenges. *J. Energy Storage* **2023**, *58*, 106347. [CrossRef]
25. Abdessadak, A.; Ghennioui, H.; Thirion-Moreau, N.; Elbhiri, B.; Abraim, M.; Merzouk, S. Digital twin technology and artificial intelligence in energy transition: A comprehensive sys-tematic review of applications. *Energy Rep.* **2025**, *13*, 5196–5218. [CrossRef]
26. Sadeghian-Jahromi, M.; Fotuhi-Firuzabad, M.; Fattaheian-Dehkordi, S.; Wang, F.; Lehtonen, M. Simultaneous planning of distribution automation and battery energy storage systems for improving resilience of distribution network. *Sustain. Energy Grids Netw.* **2025**, *42*, 101709. [CrossRef]
27. Yasir, K.; Shen, J.; Lin, J. Sustainable logistics: Synergizing passive design and pv–battery systems for carbon footprint reduction. *Buildings* **2024**, *14*, 3257. [CrossRef]
28. Symeonidou, M.M.; Zioga, C.; Papadopoulos, A.M. Life cycle cost optimization analysis of battery storage system for residential photovoltaic panels. *J. Clean. Prod.* **2021**, *309*, 127234. [CrossRef]
29. Förstl, M.; Azuatalam, D.; Chapman, A.; Verbič, G.; Jossen, A.; Hesse, H. Assessment of residential battery storage systems and operation strategies considering battery aging. *Int. J. Energy Res.* **2020**, *44*, 718–731. [CrossRef]
30. Rahman, T.; Mansur, A.A.; Hossain Lipu, M.S.; Rahman, M.S.; Ashique, R.H.; Houran, M.A.; Elavarasan, R.M.; Hossain, E. Investigation of degradation of solar photovoltaics: A review of aging factors, impacts, and future directions toward sustainable energy management. *Energies* **2023**, *16*, 3706. [CrossRef]
31. Terkes, M.; Demirci, A.; Gokalp, E.; Cali, U. Impact analysis of battery control strategies on battery aging for grid-connected and solar-powered residential battery applications. *Heliyon* **2025**, *11*, e42903. [CrossRef]
32. Longo, S.; Rincione, R.; Cellura, M.; Rossi, F.; Sinicropi, A.; Parisi, M.L. Life cycle assessment of concen-trating solar power systems and concentrating photovoltaic systems: A review. *Energy Rep.* **2025**, *14*, 4526–4539. [CrossRef]
33. Tikkiwal, V.A.; Singh, S.V.; Gupta, H.O. Multi-objective optimisation of a grid-connected hybrid PV-battery system considering battery degradation. *Int. J. Sustain. Eng.* **2021**, *14*, 1769–1779. [CrossRef]

34. Lubello, P.; Papi, F.; Bianchini, A.; Carcasci, C. Considerations on the impact of battery ageing estimation in the optimal sizing of solar home battery systems. *J. Clean. Prod.* **2021**, *329*, 129753. [CrossRef]
35. Hoppmann, J.; Volland, J.; Schmidt, T.S.; Hoffmann, V.H. The economic viability of battery storage for residential solar photovoltaic systems–A review and a simulation model. *Renew. Sustain. Energy Rev.* **2014**, *39*, 1101–1118. [CrossRef]
36. Wang, Z.; Luther, M.; Horan, P.; Matthews, J.; Liu, C. Technical and economic analyses of PV battery systems considering two different tariff policies. *Sol. Energy* **2024**, *267*, 112189. [CrossRef]
37. Padmawansa, N.; Gunawardane, K.; Madanian, S.; Than Oo, A.M. Battery energy storage capacity estimation for microgrids using digital twin concept. *Energies* **2023**, *16*, 4540. [CrossRef]
38. Ebrahimi, S.; Seyedi, M.; Ullah, S.S.; Ferdowsi, F. Resilient space operations with digital twin for solar PV and storage. *IEEE Open Access J. Power Energy* **2024**, *11*, 624–636. [CrossRef]
39. Rojek, I.; Mikołajewski, D.; Mroziński, A.; Macko, M. Machine learning-and artificial intelligence-derived prediction for home smart energy systems with PV installation and battery energy storage. *Energies* **2023**, *16*, 6613. [CrossRef]
40. Sabeel, K.; Aggarwal, G.; Siddiqui, A.M.; Ushasree, P.M.; Ali, U. Design and Optimization of Hybrid Re-newable Energy Microgrid in the UK. In *Proceedings of the 2024 IEEE International Conference on Omni-layer Intelligent Systems (COINS)*; IEEE: New York, NY, USA, 2024; pp. 1–7. [CrossRef]
41. Duan, Y.; Zhao, Y.; Hu, J. An initialization-free distributed algorithm for dynamic economic dispatch prob-lems in microgrid: Modeling, optimization and analysis. *Sustain. Energy Grids Netw.* **2023**, *34*, 101004. [CrossRef]
42. Moreno-Castro, J.; Ocaña Guevara, V.S.; León Viltre, L.T.; Gallego Landera, Y.; Cuaresma Zevallos, O.; Aybar-Mejía, M. Microgrid management strategies for economic dispatch of electricity using model predictive control techniques: A review. *Energies* **2023**, *16*, 5935. [CrossRef]
43. Shezan, S.A.; Ishraque, M.F.; Shafiullah, G.M.; Kamwa, I.; Paul, L.C.; Muyeen, S.M.; Nss, R.; Saleheen, M.Z.; Kumar, P.P. Optimization and control of solar-wind islanded hybrid microgrid by using heuristic and deter-ministic optimization algorithms and fuzzy logic controller. *Energy Rep.* **2023**, *10*, 3272–3288. [CrossRef]
44. Wang, J.; Purewal, J.; Liu, P.; Hicks-Garner, J.; Soukazian, S.; Sherman, E.; Sorenson, A.; Vu, L.; Tataria, H.; Verbrugge, M.W. Degradation of lithium ion batteries employing graphite negatives and nickel–cobalt–manganese oxide+ spinel manganese oxide positives: Part 1, aging mechanisms and life estimation. *J. Power Sources* **2014**, *269*, 937–948. [CrossRef]
45. Liu, Z.; Wang, X.; Yang, K.; Zhang, F. Analytical model of rainflow-based cyclic aging for economic battery dispatch optimization. *IEEE Trans. Energy Convers.* **2024**, *39*, 2425–2438. [CrossRef]
46. Rao, P.V.L.N.; Lavanya, V.; Manasa, D.; Boggavarapu, S.; Soni, B.P. Battery Models and Estimation Techniques for Energy Storage Systems in Residential Buildings. *J. Mod. Technol.* **2024**, *1*, 47–58. [CrossRef]
47. Baskin, I.; Ein-Eli, Y. Electrochemoinformatics as an emerging scientific field for designing materials and electrochemical energy storage and conversion devices—an application in battery science and technology. *Adv. Energy Mater.* **2022**, *12*, 2202380. [CrossRef]
48. Graner, M.; Tanjavooru, V.T.; Jossen, A.; Hesse, H. Dispatch optimi-zation of battery energy storage systems considering degradation effects and capacity inhomogeneities in second life batteries. In *International Renewable Energy Storage and Systems Conference (IRES 2023)*; 2024, July; At-Lantis Press: Dordrecht, The Netherlands, 2023; pp. 20–27. [CrossRef] [PubMed]
49. Ioannou, I.; Javaid, S.; Tan, Y.; Vassiliou, V. A Hierarchical Predictive-Adaptive Control Framework for State-of-Charge Balancing in Mini-Grids Using Deep Reinforcement Learning. *Electronics* **2025**, *15*, 61. [CrossRef]
50. Anand, A.; Loew, S.; Bottasso, C.L. Economic control of hybrid energy systems composed of wind turbine and battery. In *Proceedings of the 2021 European Control Conference (ECC) 29 June 2021*; IEEE: New York, NY, USA, 2021; pp. 2565–2572. [CrossRef]
51. Yang, H.; Yin, Y.; Abu-Siada, A. A Comprehensive Review of Solar Panel Perfor-mance Degradation and Adaptive Mitigation Strategies. *IET Control Theory Appl.* **2025**, *19*, e70040. [CrossRef]
52. Mugyema, M.; Botha, C.D.; Kamper, M.J.; Wang, R.J.; Sebitosi, A.B. Levelised cost of storage comparison of energy storage systems for use in primary response application. *J. Energy Storage* **2023**, *59*, 106573. [CrossRef]
53. Khanahmadi, A.; Mozaffarilegha, M.; Manthouri, M.; Ghaffarpour, R. A novel economic method of battery modeling in stand-alone renewable energy systems to reduce life cycle costs. *J. Energy Storage* **2021**, *44*, 103422. [CrossRef]
54. Migliari, L.; Cocco, D.; Petrollese, M. Levelized cost of storage (LCOS) of battery energy storage systems (BESS) deployed for photovoltaic curtailment mitigation. *Energies* **2025**, *18*, 3602. [CrossRef]
55. Kosmadakis, I.E.; Elmasides, C. A sizing method for PV–battery–generator systems for off-grid applications based on the LCOE. *Energies* **2021**, *14*, 1988. [CrossRef]
56. Chen, Q.; Wang, J.; Cang, M.; Zhai, X.; Cheng, X.; Wu, S.; Li, D. Optimal scheduling of a township integrated-energy system using the adjustable heat-electricity ratio model. *Glob. Energy Interconnect.* **2024**, *7*, 48–60. [CrossRef]
57. Eskandari, A.; Emamian, M.; Nedaei, A.; Aghaei, M. Digital twin technology in microgrid systems. In *Digital Twin Technology for the Energy Sector*; Elsevier: Amsterdam, The Netherlands, 2025; pp. 111–141. [CrossRef]

58. Hosseini, E.; Horrillo-Quintero, P.; Carrasco-Gonzalez, D.; Garcia-Trivino, P.; Sarrias-Mena, R.; Garcia-Vazquez, C.A.; Fernandez-Ramirez, L.M. Reinforcement learning-based energy management system for lithium-ion battery storage in multilevel microgrid. *J. Energy Storage* **2025**, *109*, 115114. [CrossRef]
59. Sangoleye, F.; Jao, J.; Faris, K.; Tsiropoulou, E.E.; Papavassiliou, S. Reinforcement learning-based demand response management in smart grid systems with prosumers. *IEEE Syst. J.* **2023**, *17*, 1797–1807. [CrossRef]
60. Rehman, U.U. Proximal policy optimization–driven real-time home energy man-agement system with storage and renewables. *Process Integr. Optim. Sustain.* **2025**, *9*, 507–536. [CrossRef]
61. Mohammadi, P.; Darshi, R.; Shamaghdari, S.; Siano, P. Comparative Analysis of Control Strategies for Microgrid Energy Management with a Focus on Reinforcement Learning. *IEEE Access* **2024**, *12*, 171368–171395. [CrossRef]
62. Chicaiza, W.D.; Topa, A.O.; Sánchez, A.J.; Escaño, J.M.; Álvarez, J.D. Model design for photovoltaic facilities based on fuzzy neural network as core of its digital twin. *Energy Convers. Manag.* **2025**, *342*, 120001. [CrossRef]
63. Yao, J.; Billings, B.; Gao, T.; Hedengren, J.; Powell, K.M. Optimal sizing of battery energy storage systems for peak shaving and demand response using a degradation-aware Bayesian Optimi-zation-Mixed-Integer Linear Programming framework. *Energy Convers. Manag.* **2026**, *350*, 120947. [CrossRef]
64. Khan, B.; Ali, S.M.; Ullah, Z. Deep learning based digital twins augmented reality: Model predictive control for battery and storage optimization in renewable energy prosumers districts. *J. Energy Storage* **2025**, *131*, 117565. [CrossRef]
65. Salaorni, D.; Bianchi, F.; Colnago, S.; Barisione, A.; Trovò, F.; Restelli, M. A novel digital twin for battery energy storage systems in micro-grids. *J. Energy Storage* **2025**, *132*, 117745. [CrossRef]
66. Zheng, X.; Ju, C.; Yang, G.; Chu, J. Risk-aware collaborative optimization for quantity–price bidding and energy storage dispatch in virtual power plants. *J. Energy Storage* **2026**, *149*, 120112. [CrossRef]
67. Meng, Q.; He, Y.; Hussain, S.; Lu, J.; Guerrero, J.M. Design and optimization of solar photovoltaic microgrids with adaptive storage control for residential standalone systems. *Energy Rep.* **2025**, *14*, 989–997. [CrossRef]
68. Zou, Y.; Yang, Y.; Zhang, Y.; Liu, C. Aging-aware co-optimization of topology, pa-rameter and control for multi-mode input-and output-split hybrid electric powertrains. *J. Power Sources* **2024**, *624*, 235564. [CrossRef]
69. Hassan, A.; Hollweg, G.V.; Su, W.; Zhou, X.; Wang, M. Degradation-Aware Bi-Level Optimization of Second-Life Battery Energy Storage System Considering Demand Charge Reduc-tion. *Energies* **2025**, *18*, 3894. [CrossRef]
70. Slaifstein, D.; Mouli, G.R.C.; Ramirez-Elizondo, L.; Bauer, P. Ageing-aware energy management for residential multi-carrier energy systems. *J. Energy Storage* **2026**, *173*, 122889. [CrossRef]
71. Butt, H.Z.; Li, X. Enhancing optimal microgrid planning with adaptive BESS degra-dation costs and PV asset management: An iterative post-optimization correction framework. *Electr. Power Syst. Res.* **2025**, *247*, 111785. [CrossRef]
72. Safavi, V.; Vaniar, A.M.; Bazmohammadi, N.; Vasquez, J.C.; Keysan, O.; Guerrero, J.M. A battery degradation-aware energy management system for agricultural microgrids. *J. Energy Storage* **2025**, *108*, 115059. [CrossRef]
73. Nnorom, O.; Ogut, M.G.; Boyd, S.; Levis, P. Aging-aware battery control via convex optimization. *Optim. Eng.* **2026**, *27*, 1303–1326. [CrossRef]
74. Schade, C.; Egging-Bratseth, R. Battery degradation: Impact on economic dis-patch. *Energy Storage* **2024**, *6*, e588. [CrossRef]
75. Durowoju, E.; Salaudeen, H. Advancing lifecycle-aware battery architectures with embedded self-healing and recyclability for sustainable high-density renewable energy storage applications. *World J. Adv. Res. Rev.* **2022**, *14*, 744–765. [CrossRef]
76. Sivaneasan, B.; Tan, K.T.; Zhang, W. Cognitive Digital Twins for the Microgrid: A Real-World Study for Intelligent Energy Management and Optimization. *IEEE Internet Comput.* **2025**, *29*, 39–47. [CrossRef]
77. Gilabert-Torres, C.; Escrig-Sos, J.; García-Díaz, J.C.; Quiles-Carrillo, L. Photovoltaic systems with battery storage: A comprehensive scheduling method for high-consumption facili-ties. *J. Energy Storage* **2025**, *112*, 118858. [CrossRef]
78. Ding, X.; Liu, Y.; Zhang, Y.; Wang, J. Dual-module coupled rolling optimization for hy-dro–wind–PV–battery complementary systems, considering battery capacity degradation. *J. Energy Storage* **2025**, *111*, 118104. [CrossRef]
79. Shah, S.A.; Shah, S.M.; Wang, S.; Niazi, S.G.; Xu, Z.; Wu, M. A review of attention-enhanced deep-learning models for state of charge estimation in lithium-ion batteries: Current progress and future directions. *J. Energy Storage* **2026**, *154*, 121207. [CrossRef]
80. Yan, Y.; Meng, J.; Song, Z.; Zhang, S.; Pan, Y.; Peng, Q.; Peng, J. A multi-stress universal degradation framework for lithium-ion batteries in diverse energy storage scenarios. *J. Energy Storage* **2026**, *154*, 121305. [CrossRef]
81. Elseify, M.; El-Shimy, M.; Mohamed, E.A.; Siano, P. Optimal scheduling of photovoltaic and battery energy storage in distribution networks using an ameliorated sand cat swarm optimisation algorithm: Economic assessment with different loading scenarios. *J. Energy Storage* **2025**, *110*, 116026. [CrossRef]
82. Liu, Z.; Chen, Y.; Wang, X.; Zhang, F. An energy collaboration framework considering community energy storage and PV charging station clusters. *J. Energy Storage* **2025**, *109*, 115976. [CrossRef]
83. Athanasiadis, C.L.; Papadopoulos, T.A.; Kryonidis, G.C.; Doukas, D.I. A holistic and personalized home energy management system with non-intrusive load monitoring. *IEEE Trans. Consum. Electron.* **2024**, *70*, 6725–6737. [CrossRef]

84. European Commission Joint Research Centre. *PVGIS: Photovoltaic Geographical Information System [Internet]*; European Commission Joint Research Centre: Ispra, Italy, 2024. Available online: https://re.jrc.ec.europa.eu/pvg_tools/en/ (accessed on 26 February 2026).
85. Rezaeimozafar, M.; Barrett, E.; Monaghan, R.F.; Duffy, M. A stochastic method for behind-the-meter PV-battery energy storage systems sizing with degradation minimization by limiting battery cycling. *J. Energy Storage* **2024**, *86*, 111199. [CrossRef]

Disclaimer/Publisher's Note: The statements, opinions and data contained in all publications are solely those of the individual author(s) and contributor(s) and not of MDPI and/or the editor(s). MDPI and/or the editor(s) disclaim responsibility for any injury to people or property resulting from any ideas, methods, instructions or products referred to in the content.